NASA Technical Memorandum 87769

NASA-TM-87769 19860020305

AN ENTROPY CORRECTION METHOD FOR UNSTEADY FULL POTENTIAL FLOWS WITH STRONG SHOCKS

WOODROW WHITLOW, JR.
MOHAMED M. HAFEZ
STANLEY J. OSHER

JUNE 1986

NASA

National Aeronautics and
Space Administration

Langley Research Center
Hampton, Virginia 23665

NF01641

AN ENTROPY CORRECTION METHOD FOR UNSTEADY FULL POTENTIAL FLOWS WITH STRONG SHOCKS

Woodrow Whitlow, Jr.*
NASA Langley Research Center
Hampton, Virginia 23665-5225

Mohamed M. Hafez**
University of California, Davis
Davis, CA 95616

Stanley J. Osher***
University of California, Los Angeles
Los Angeles, CA 90024

Abstract

An entropy correction method for the unsteady full potential equation is presented. The unsteady potential equation is modified to account for entropy jumps across shock waves. The conservative form of the modified equation is solved in generalized coordinates using an implicit, approximate factorization method. A flux-biasing differencing method, which generates the proper amounts of artificial viscosity in supersonic regions, is used to discretize the flow equations in space. Comparisons between the present method and solutions of the Euler equations and between the present method and experimental data are presented. The comparisons show that the present method more accurately models solutions of the Euler equations and experiment than does the isentropic potential formulation.

Nomenclature

a	speed of sound
A_1, A_2, A_3	metrics of coordinate transformation, Equation (7)
c	airfoil chord
h	time step in computational space
i, j	indices of grid points
I	identity matrix
J	Jacobian of coordinate transformation
k	reduced frequency based on semichord
M	Mach number
q	total speed
r	distance from point of rotation to a point in the flow field
R	gas constant
s	entropy
t	time
U, W	contravariant velocities, Equation (6)
x, z	cartesian coordinates
α	angle of attack
β	$\rho^{2-\gamma}/J$
γ	ratio of specific heats
Γ	jump in potential across the wake
δ	difference operator
ξ, ζ	computational coordinate directions
θ	polar angle
θ_s	airfoil pitch angle
ρ	density
$\bar{\rho}$	ρ/J
$\tilde{\rho}$	biased density
τ	computational time
ϕ	velocity potential
$\langle \rangle$	average of quantity across the wake

Subscripts

i	isentropic
n	normal to shock
o	steady airfoil location
p	pitch axis location
s	points on airfoil
1	minimum airfoil pitch angle
2	maximum airfoil pitch angle
∞	free stream conditions

Superscripts

ℓ	lower side of wake
n	iteration number
u	upper side of wake
$*$	sonic conditions

*Research Scientist, Unsteady Aerodynamics Branch, Loads and Aeroelasticity Division, Member AIAA.
**Professor of Mechanical Engineering, Associate Fellow AIAA.
***Professor of Mathematics, Member AIAA.

Introduction

Modern aircraft typically operate at high speeds where aeroelastic instabilities are more likely to occur. To successfully predict and analyze such aeroelastic phenomena, the aircraft designer needs methods that accurately predict the aerodynamic loads--steady and unsteady--that the vehicle experiences. Since many critical aeroelastic phenomena occur at transonic speeds, methods based on linear aerodynamic theory cannot accurately predict many aeroelastic responses. Thus, it is necessary to use an aerodynamic method that can predict time-accurate solutions of nonlinear flows and that can accurately model shock waves and their unsteady motions.

When shock waves appear in transonic flow fields, aerodynamic loads predicted using potential flow theory can be grossly inaccurate and even multivalued. Multiple solutions of the potential equation were first observed in two dimensions by Steinhoff and Jameson.[1] Salas and Gumbert[2] showed that the phenomenon is not

confined to a particular airfoil or flow condition. Williams et al.[3] calculated multiple solutions using two-dimensional (2-D) transonic small disturbance (TSD) theory. Gibbons et al.[4] showed multiple solutions for three-dimensional (3-D) TSD calculations on high-aspect-ratio wings. For lower aspect ratios, multiple solutions were not observed, but calculated lift coefficients were highly inaccurate when shock waves were in the flow field.

Since potential theory can yield inaccurate transonic aerodynamic loads, aeroelastic analysis performed using these loads has to be considered unreliable. The inaccuracy is primarily a result of potential theory not modeling the jump in entropy that a fluid particle experiences as it passes through a shock wave. Therefore, calculated shock waves can have the wrong strength and be in the wrong location.

Currently, the most widely used methods for unsteady, nonlinear flow analysis are based on TSD theory.[5-7] Fuglsang and Williams[8] modeled the effects of entropy jumps through shock waves in 2-D TSD theory; Gibbons et al.[4] extended that method to three dimensions. These efforts resulted in TSD methods that more closely model solutions of the Euler equations than does isentropic TSD theory.

However, TSD theory has some significant limitations. Only flows past bodies of small thicknesses at small angles of incidence and undergoing small amplitude unsteady motions can be analyzed. In addition, the TSD equations are formulated assuming that the free stream Mach number is near unity. Because of these limitations, the purpose of the present effort is to develop an improved method for predicting nonlinear, unsteady aerodynamic loads on 2-D bodies. A primary objective of this effort is to model the nonisentropic effects caused by shock waves.

The present method is based on the unsteady full potential equation. Hafez and Lovell[9] presented a method for modeling entropy jumps across shock waves in steady potential flows. They showed that by modifying the isentropic density to include the effects of entropy jumps across shocks, steady potential solutions closer to Euler solutions are obtained. In the present effort, Hafez's and Lovell's method is extended to unsteady flows.

A flux-biasing differencing method[10,11] is used to discretize the flow equations and to model shock discontinuities. To increase computational efficiency, grids for unsteady calculations are generated, at each time step, using linear interpolation between grids calculated at extreme airfoil positions.

Problem Formulation

Governing Equations

The formulation used in the present effort is that presented by Bridgeman et al.[12] The flow field is described by the two-dimensional, unsteady full potential equation in conservation form

$$\rho_t + (\rho\phi_x)_x + (\rho\phi_z)_z = 0 \qquad (1)$$

where ϕ is the velocity potential, and density ρ is determined from Bernoulli's equation

$$\rho = [1 + \frac{\gamma-1}{2}(M_\infty^2 - 2\phi_t - \phi_x^2 - \phi_z^2)]^{\frac{1}{\gamma-1}} \qquad (2)$$

The spatial coordinates, x and z, are normalized by airfoil chord c, and time t is normalized by a_∞/c, where a_∞ is the free stream speed of sound. Density is normalized by the free stream density ρ_∞, and ϕ is normalized by $a_\infty c$.

A transformation to a body-fitted coordinate system is given by

$$\xi = \xi(x,z,t)$$

$$\zeta = \zeta(x,z,t) \qquad (3)$$

$$\tau = t$$

where ξ and ζ are the computational coordinate directions around and normal to the airfoil, respectively, and τ is the computational time. Strong conservation form of (1) is maintained by writing the continuity equation in transformed coordinates as

$$(\frac{\rho}{J})_\tau + (\frac{\rho U}{J})_\xi + (\frac{\rho W}{J})_\zeta = 0 \qquad (4)$$

Equation (2) transforms to

$$\rho = \{1 + \frac{\gamma-1}{2}[M_\infty^2 - 2\phi_\tau - (U+\xi_t)\phi_\xi + (W+\zeta_t)\phi_\zeta]\}^{\frac{1}{\gamma-1}} \quad (5)$$

where the contravariant velocities in the ξ and ζ directions, U and W, respectively, are given by

$$U = \xi_t + A_1\phi_\xi + A_2\phi_\zeta$$

$$W = \zeta_t + A_2\phi_\xi + A_3\phi_\zeta \qquad (6)$$

The metric terms are

$$A_1 = \xi_x^2 + \xi_z^2$$

$$A_2 = \xi_x\zeta_x + \xi_z\zeta_z \qquad (7)$$

$$A_3 = \zeta_x^2 + \zeta_z^2$$

and the Jacobian of the transformation J is

$$J = \xi_x\zeta_z - \xi_z\zeta_x \qquad (8)$$

Approximate Factorization

Equation (4) is solved using first order backward differencing in time and second order central differencing in space as in reference 12. The time derivative of density is linearized about previous time levels such that conservation form is maintained. The resulting equation is approximately factored into the form $L_\xi L_\zeta \Delta\phi = F$. This becomes

2

$$[I + hU^n\delta_\xi - \frac{h^2}{\beta^n}\delta_\xi(\bar{\rho}A_1)^n\delta_\xi]$$

$$\times [I + hW^n\delta_\zeta - \frac{h^2}{\beta^n}\delta_\zeta(\bar{\rho}A_3)^n\delta_\zeta](\phi^{n+1} - \phi^n)$$

$$= (\phi^n - \phi^{n-1}) + \frac{\beta^{n-1}}{\beta^n}(\phi^n - 2\phi^{n-1} + \phi^{n-2})$$

$$+ \frac{h}{\beta^n}(\bar{\rho}^n - \bar{\rho}^{n-1})$$

$$+ h\frac{\beta^{n-1}}{\beta^n}(U^{n-1}\delta_\xi + W^{n-1}\delta_\zeta)(\phi^n - \phi^{n-1})$$

$$+ \frac{h^2}{\beta^n}[\delta_\xi(\frac{\tilde{\rho}U}{J})^n + \delta_\zeta(\bar{\rho}W)^n - F_\infty] \qquad (9)$$

where

$$L_\xi = [I + hU^n\delta_\xi - \frac{h^2}{\beta^n}\delta_\xi(\bar{\rho}A_1)^n\delta_\xi]$$

$$L_\zeta = [I + hW^n\delta_\zeta - \frac{h^2}{\beta^n}\delta_\zeta(\bar{\rho}A_3)^n\delta_\zeta]$$

$$\Delta\phi = \phi^{n+1} - \phi^n$$

and F represents the right side of (9). In (9), δ_ξ and δ_ζ represent central difference operators, the superscripts n, n-1, and n+1 represent time levels,

$$h = \Delta\tau$$

$$\bar{\rho} = \frac{\rho}{J}$$

$$\beta = \frac{\rho^{2-\gamma}}{J}$$

The density biased in the ξ direction is given by $\tilde{\rho}$, and F_∞ is a correction to the residual due to incomplete metric cancellation.[12,13]

Airfoil Boundary Conditions

The flow is required to be tangent to the airfoil boundary. This condition is imposed by requiring

$$W = \zeta_t + A_2\phi_\xi + A_3\phi_\zeta = 0 \qquad (10)$$

at the airfoil. Equation (10) is applied as

$$(\phi_\zeta)_{i,J} = -(\frac{A_2}{A_3}\phi_\xi)_{i,J} - (\frac{\zeta_t}{A_3})_{i,J} \qquad (11)$$

where the subscript J represents points on the body. The tangency condition implies that

$$(\bar{\rho}W)_{i,J-1/2} = -(\bar{\rho}W)_{i,J+1/2} \qquad (12)$$

Using (11) and (12), the flow tangency condition is imposed implicitly on both sides of (9) by changing the L_ξ and L_ζ operators to

$$L_\xi = [I + hU^n\delta_\xi - \frac{h^2}{\beta^n}\delta_\xi\bar{\rho}^n(A_1 - \frac{A_2^2}{A_3})^n\delta_\xi]$$

$$L_\zeta = [I - \frac{2h^2}{\beta^n}\delta_\zeta(\bar{\rho}A_3)^n\delta_\zeta]$$

and by representing the $\delta_\zeta(\bar{\rho}W)$ term on the right side as $2(\bar{\rho}W)_{i,J+1/2}$.

Dynamic Grids

To apply the flow tangency condition at the instantaneous surface position of moving airfoils requires a new grid at each time step. Since the resources needed to compute these grids using an elliptic method[14] can be more than those necessary to do the aerodynamic calculations, an efficient interpolation method is used to generate the required grids. To simulate harmonic motions, the elliptic method[14] is used to calculate grids at the extremes of the motion. Grids for all other airfoil positions are then generated using interpolation. Interior grid points are redistributed at each time step, while points on the outer boundary remain fixed.

The method is illustrated in figure 1 for an airfoil pitching about a point x_p. A polar coordinate system centered at x_p is used. Using the subscripts 1 and 2 to denote the minimum and maximum pitch angles, the position of a grid point at any time τ is given by

$$r(\tau) = r_1 + \frac{\theta_s(\tau) - \theta_{s1}}{\theta_{s2} - \theta_{s1}}(r_2 - r_1) \qquad (13)$$

$$\theta(\tau) = \theta_1 + \frac{\theta_s(\tau) - \theta_{s1}}{\theta_{s2} - \theta_{s1}}(\theta_2 - \theta_1) \qquad (14)$$

where $\theta_s(\tau)$ is the instantaneous airfoil pitch angle,

$$r_1 = (x_1^2 + z_1^2)^{\frac{1}{2}}$$

$$r_2 = (x_2^2 + z_2^2)^{\frac{1}{2}}$$

$$\theta_1 = \tan^{-1}(\frac{z_1}{x_1})$$

$$\theta_2 = \tan^{-1}(\frac{z_2}{x_2})$$

Interpolated grid points are then given by

$$x(\tau) = r(\tau)\cos\theta(\tau)$$

$$z(\tau) = r(\tau)\sin\theta(\tau)$$

Points on the body, x_s and z_s, are defined at each instant by

$$x_s(\tau) = x_p + (x_o - x_p)\cos\theta_s(\tau) + z_o\sin\theta_s(\tau)$$

$$z_s(\tau) = \qquad - (x_o - x_p)\sin\theta_s(\tau) + z_o\cos\theta_s(\tau)$$

where the subscript o represents steady state locations. The time-dependent metric terms

$$\xi_t = -x_\tau\xi_x - z_\tau\xi_z$$

$$\zeta_t = -x_\tau\zeta_x - z_\tau\zeta_z$$

are then computed using first order differences for x_τ and z_τ.

To demonstrate the interpolation method, figure 2 shows grids for an airfoil pitching about its quarter chord and the angle of attack $\alpha(\tau)$ given by $\alpha(\tau) = 22.5°(1 + \sin(k\tau))$. The calculated grids for $\alpha(\tau) = 0°$ and $45°$ are shown in figures 2a and 2d, respectively; they were generated with the GRAPE program[14] which uses an elliptic method. The interpolated grids for $\alpha(\tau) = 15°$ and $30°$ are shown in figures 2b and 2c. Even for such large angles, the interpolation works successfully. The details of the near-field grids cannot be seen, but the grids remain near orthogonal; the metric A_2, which is a measure of the skewness of the grids is much smaller than A_1 and A_3 over the entire grid. If $A_2 = 0$ everywhere, the grid would be perfectly orthogonal. Grid lines intentionally were not plotted across the wakes to make those regions easy to identify.

Unsteady Wake Condition

For lifting flows, the shed vorticity is represented as a jump in potential across a wake line. The following wake boundary condition[12] is used in the present effort

$$\Gamma_\tau + \langle W\rangle\Gamma_\zeta = 0 \qquad (15)$$

where Γ is the jump in potential across the wake, $\phi^u - \phi^\ell$, and $\langle W\rangle$ is the average of W above and below the wake, $1/2(W^u + W^\ell)$. The unsteady transport condition for the jump in potential, (15), is obtained by assuming that the isentropic density and normal velocity are continuous across the wake. It does not model the jump in entropy across the wake that can result when shocks of different strengths are on the upper and lower surfaces. However, Hafez and Lovell[9] have demonstrated that assuming the isentropic density to be continuous across the wake is a good approximation for the full potential formulation with entropy corrections.

Far-Field Conditions

In the far field, the flow is set to free stream conditions

$$\phi = M_\infty x$$

$$\rho = 1$$

where M_∞ is the free stream Mach number.

Flux Biasing

The residual terms on the right side of (9) are centrally differenced about the node point (i,j) to give

$$\delta_\xi\left(\frac{\tilde{\rho}U}{J}\right)_{i,j} = \left(\frac{\tilde{\rho}U}{J}\right)_{i+1/2,j} - \left(\frac{\tilde{\rho}U}{J}\right)_{i-1/2,j}$$

$$\delta_\zeta(\bar{\rho}W)_{i,j} = (\bar{\rho}W)_{i,j+1/2} - (\bar{\rho}W)_{i,j-1/2}$$

The computational cell is shown in figure 3. In supersonic regions, artificial viscosity, necessary to capture shocks, is introduced by biasing the density in the upwind direction. Although it is generally necessary to upwind the density in both computational directions, in this work, upwinding only in the ξ direction has been found to be satisfactory. The biased density $\tilde{\rho}$ is defined as (for $U > 0$)

$$\tilde{\rho}_{i+1/2,j} = \frac{1}{q_{i+1/2,j}}[\rho q - \Delta\xi(\rho q)_\xi^-]_{i+1/2,j}$$

$$= \frac{1}{q_{i+1/2,j}}[(\rho q)_{i+1/2,j} - (\rho q)_{i+1/2,j}^-$$

$$+ (\rho q)_{i-1/2,j}^-] \qquad (16)$$

where

$$(\rho q)^- = \rho q - \rho^* q^* \qquad q > q^* \qquad (17)$$

$$0 \qquad q < q^*$$

q is the flow speed ($q^2 = \phi_x^2 + \phi_z^2$), and q^* and ρ^* are the sonic speed and density, respectively, given by

$$q^{*2} = \frac{2}{\gamma+1}[1 + \frac{\gamma-1}{2}(M_\infty^2 - 2\phi_\tau - 2\xi_t\phi_\xi - 2\zeta_t\phi_\zeta)] \qquad (18)$$

$$\rho^* = (q^{*2})^{\frac{1}{\gamma-1}} \qquad (19)$$

For steady flows, ρ^* and q^* are constants that are computed once, but for unsteady flows, ρ^* and q^* must be computed at each grid point at every time step.

Flux biasing is an improvement upon density biasing since it (a) accurately tracks sonic conditions and requires no empirical constants to specify the amount of artificial viscosity, (b) produces no velocity overshoots at shock waves, thus allowing for larger time steps--increasing computational efficiency--for unsteady calculations, (c) produces well defined, monotone shock profiles with a maximum two point transition between the upstream and downstream states, and (d) dissipates expansion shocks, ruling out solutions with such nonphysical characteristics. Shankar[15,16] has previously used flux biasing in unsteady full potential calculations.

4

Entropy Correction Method

When a fluid particle passes through a shock wave, it experiences a jump in entropy. The entropy jump Δs is a function of the normal Mach number upstream of the shock M_n

$$\frac{\Delta s}{R} = \frac{1}{\gamma-1}\{\ln(\frac{2\gamma}{\gamma+1}M_n^2 - \frac{\gamma-1}{\gamma+1}) - \gamma\ln[\frac{(\gamma+1)M_n^2}{(\gamma-1)M_n^2 + 2}]\} \tag{20}$$

For unsteady flows, the shock speed must be monitored to obtain the speed of the flow relative to the shock. Here, the entire shock is assumed to move at the same speed as the base of the shock. To account for the entropy jump, the density is modified to

$$\rho = \rho_i e^{\frac{-\Delta s}{R}} \tag{21}$$

where the isentropic density, ρ_i, is given by (5). Expanding the continuity equation, (1), yields

$$e^{\frac{-\Delta s}{R}}[\rho_{i_t} + (\rho_i\phi_x)_x + (\rho_i\phi_z)_z] -$$

$$\rho_i e^{\frac{-\Delta s}{R}}[(\frac{\Delta s}{R})_t + u(\frac{\Delta s}{R})_x + w(\frac{\Delta s}{R})_z] = 0 \tag{22}$$

where $u = \phi_x$, and $w = \phi_z$. The last part of (22) vanishes since $\frac{Ds}{Dt} = 0$ in the isentropic flow regions. The remaining part of (22) is the classical potential equation except across shock waves and wakes where there is a jump in entropy. Hafez and Lovell[9] showed that assuming the isentropic pressure to be continuous across the wake is a good approximation except near the trailing edge. Thus, that assumption is made here, and the wake condition in (15) is used for all nonisentropic calculations.

To implement the entropy corrections, the difference operator at shock points is modified. Equation (4) is discretized as

$$\frac{\bar{\rho}_{i,j}^{n+1} - \bar{\rho}_{i,j}^{n}}{h} + (\frac{\tilde{\rho U}}{J})_{i+1/2,j}^{n+1} - (\frac{\tilde{\rho U}}{J})_{i-1/2,j}^{n+1}$$

$$+ (\bar{\rho}W)_{i,j+1/2}^{n+1} - (\bar{\rho}W)_{i,j-1/2}^{n+1} = 0 \tag{23}$$

At shock points, (23) is modified to

$$[(\bar{\rho}_i e^{\frac{-\Delta s}{R}})_{i,j}^{n+1} - (\bar{\rho}_i e^{\frac{-\Delta s}{R}})_{i,j}^{n}]\frac{1}{h}$$

$$+ (\frac{\tilde{\rho U}}{J})_{i+1/2,j}^{n+1} - (\frac{\tilde{\rho U}}{J})_{i-1/2,j}^{n+1}$$

$$+ (\bar{\rho}e^{\frac{-\Delta s}{R}}W)_{i,j+1/2} - (\bar{\rho}e^{\frac{-\Delta s}{R}}W)_{i,j-1/2} = 0 \tag{24}$$

where Δs is a function of $M_{n_{i-3/2,j}}$, and

$$\tilde{\rho}_{i+1/2,j} = (\rho_i e^{\frac{-\Delta s}{R}})_{i+1/2,j} +$$

$$\frac{1}{q_{i+1/2,j}}(\rho_i q - \rho^* q^*)_{i-1/2,j} \tag{25}$$

The computational cell at shock points is shown in figure 4. In the approximate factorization scheme, this is implemented by representing

the $\frac{h}{\beta^n}(\bar{\rho}^n - \bar{\rho}^{n-1})$ and $\frac{h^2}{\beta^n}[\delta_\xi(\frac{\tilde{\rho U}}{J}) + \delta_\zeta(\bar{\rho}W)]$

terms in (9) as

$$\frac{h}{\beta^n}[(\bar{\rho}_i e^{\frac{-\Delta s}{R}})_{i,j}^n - (\bar{\rho}_i e^{\frac{-\Delta s}{R}})_{i,j}^{n-1}] \text{ and}$$

$$\frac{h^2}{\beta^n}[(\frac{\tilde{\rho U}}{J})_{i+1/2,j}^n - (\frac{\tilde{\rho U}}{J})_{i-1/2,j}^n$$

$$+ (\bar{\rho}_i e^{\frac{-\Delta s}{R}}W)_{i,j+1/2} - (\bar{\rho}_i e^{\frac{-\Delta s}{R}}W)_{i,j-1/2}],$$

respectively, where $\tilde{\rho}_{i+1/2,j}$ is given by (25). The effect of the entropy correction is to introduce a source distribution along the shock. The source strength is dependent upon Δs.

Results and Discussion

Steady pressures on an NACA 0012 airfoil have been calculated using the isentropic and nonisentropic formulations. Euler calculations[17] at the same flow conditions were also made. Unsteady pressures on the NACA 0012 oscillating in pitch about its quarter chord were computed using the isentropic and the nonisentropic methods. Comparisons of those calculated pressures with TSD calculations and with experimental data were made. The above unsteady calculations were made using grid interpolation to simulate the airfoil unsteady motion. In addition, unsteady calculations were made using grid rotation to simulate the airfoil motion. Comparisons of the unsteady results

5

obtained by the two methods were made. Steady pressures on the NLR 7301 airfoil were computed using the isentropic and the nonisentropic methods. Comparisons between the isentropic method, TSD, and experiment and between both full potential methods, Euler calculations, and experiment were made. All calculations were made using O-type grids with 101 points around the airfoil and 31 points outward from the airfoil.

NACA 0012

In this section, the calculations made for the NACA 0012 airfoil are presented. These results demonstrate the accuracy of the present isentropic potential method and the improvements that result when the effects of entropy are modeled.

Figure 5 shows the steady pressures that are calculated using the potential methods and an Euler method[17] for M_∞ = 0.84, α = 0°. For this airfoil, the flow conditions are in the region where multiple solutions are known to occur. The isentropic result in figure 5 shows an asymmetric solution with negative lift. The other possible solutions are an asymmetric solution with positive lift (the opposite of the solution in figure 5), and a symmetric solution with zero lift. The Euler solution for this case is symmetric with zero lift. When entropy corrections are used, the potential method yields a symmetric, nonlifting solution. The calculated pressure distribution agrees very well with that obtained by solving the Euler equations.[17] By modeling the shock-generated entropy, the nonphysical asymmetric solution is eliminated, and a symmetric pressure distribution is obtained.

Calculated unsteady pressures on an NACA 0012 oscillating in pitch about its quarter chord, $\alpha(\tau)$ = 0.016° + 2.51°sin($k\tau$), at M_∞ = 0.755 and k = 0.0814 are shown in figures 6a-6f. Included in the figures are isentropic full potential (FP) calculations, TSD calculations made using the code of reference 6, and experimental data.[18] The instantaneous pressure distributions show that the present method agrees very well with experiment over the entire range of unsteady motion. These calculations show the increased accuracy that is obtained by going from TSD theory to full potential and applying the flow tangency condition on the actual airfoil boundary. The most notable improvement is the accuracy of the computed pressures on the forward portion of the airfoil. The present method does a much better job of calculating the flow over this portion of the airfoil than does the TSD method. The FP shock positions and strengths show good agreement with the experimental data, although the shock waves generally are further aft and stronger than the measured shocks. This is the expected result for an isentropic potential flow method.

For improved accuracy of the FP method, the effects of shock-generated entropy are included in the calculations. The corresponding results for the case of figure 6 are shown in in figures 7a-7f. Those figures show the isentropic and nonisentropic pressures and experimental data. Generally, at each instant in the cycle of

motion, the effects of the entropy corrections are to weaken the shock and move it forward such that the nonisentropic pressures agree better with the measured data than do the isentropic pressure distributions. In figure 7d, the position and strength of the isentropic shock on the lower surface are in excellent agreement with the measured data, and the effects of entropy cause virtually no change. Including the effects of entropy generally does not result in more accurate modeling of the flow immediately downstream of shock waves. This is because the thickening of the boundary layer that occurs downstream of embedded shocks is not modeled in the inviscid formulation. At points in the cycle where the shocks become strong, the measured pressures immediately behind the shocks show the effects of boundary layer thickening.

In calculating the pressures of figures 6 and 7, the airfoil motion was simulated by interpolating the grids between the extreme airfoil positions. An attempt was made to simplify the calculations by rotating the entire grid to model the airfoil motion. The metrics were recomputed at each time step, and the airfoil boundary condition was applied at the instantaneous surface position. Examples of the unsteady pressures calculated using this procedure are shown in figures 8a and 8b. The calculations correspond to those in figures 6a and 6e, respectively. Included in the figures are experimental data and the isentropic pressures calculated by interpolating grids to simulate airfoil motion. It is seen that rotating the entire grid causes large differences in the calculated pressures and very poor agreement with the measured data. Thus for the current formulation, grid rotation should not be used. It should be noted that Malone and Sankar[19] successfully used grid rotation and translation for unsteady full potential calculations. That method uses a different linearization and different far-field boundary conditions than those used here.

NLR 7301

Steady pressures on the NLR 7301 airfoil at its design condition, M_∞ = 0.721 and α = -0.19°, are shown in figure 9. Included are isentropic FP calculations, TSD calculations, and measured pressures.[20] Again, the improved accuracy that is obtained with the full potential formulation is evident. Although the level of pressures on the upper surface is higher than the experimental values and the shock is too strong and aft of its experimental location, the present method correctly predicts the trend of the pressure distributions. The TSD method predicts two shocks on the upper surface-- one on the forward portion of the airfoil and another near the measured shock location.

Entropy corrections were applied to the case of figure 9; the results are shown in figure 10. That figure shows a comparison of the isentropic and nonisentropic FP pressures, Euler[17] pressures, and experimental data.[20] The effects of modeling the shock-generated entropy are to weaken the shock and move it forward. The level of pressures upstream of the FP shock remain higher than those of the Euler pressures and the experimental data.

Concluding Remarks

A method for modeling the effects of shock-generated entropy has been developed for the unsteady full potential equation. This was accomplished by modifying the isentropic density immediately downstream of shock waves to account for the local jump in entropy. The entropy correction method was implemented in a two-dimensional full potential code that used a flux biasing differencing method to discretize the flow equations. The resulting method was tested for steady and unsteady flow past an NACA 0012 airfoil and for steady flow past an NLR 7301 airfoil. Comparisons of the isentropic and nonisentropic calculations were made with transonic small disturbance and Euler calculations and with experimental data.

For the NACA 0012 airfoil, modeling the entropy effects alleviated the phenomenon of multiple solutions in a steady flow case. In that case, a unique solution that showed good agreement with an Euler solution was obtained. For unsteady flow, the primary effects were to weaken the shock and to cause slight changes in its location. In comparisons of the unsteady calculations with experimental data, the nonisentropic shock always moved toward the measured shock location.

Calculations for the NLR 7301 airfoil at its design condition also showed the effects of the entropy corrections to be a slight weakening and forward shift of the shock from its isentropic location. The calculated pressures show the correct trends, but the pressure levels are too high.

To summarize, the entropy correction method alleviated the phenomenon of multiple solutions in a case where it was observed. The primary effects of modeling shock-generated entropy are to weaken and cause a slight shift of the shock position.

References

[1]Steinhoff, John; and Jameson, Antony: Multiple Solutions of the Transonic Potential Flow Equation, AIAA Journal, Vol. 20, No. 11, November 1982, pp. 1521-1525.

[2]Salas, M. D.; and Gumbert, C. R.: Breakdown of the Conservative Potential Equation, AIAA Paper 85-0367.

[3]Williams, M.; Bland, S.; and Edwards, J.: Flow Instabilities in Transonic Small Disturbance Theory, NASA TM 86251, January 1985.

[4]Gibbons, M. D.; Whitlow, W., Jr.; and Williams, M. H.: Nonisentropic Unsteady Three Dimensional Small Disturbance Potential Theory, AIAA Paper 86-0863.

[5]Ballhaus, W. F.; and Goorjian, P. M.: Implicit Finite-Difference Computations of Unsteady Transonic Flows about Airfoils, AIAA Journal, Vol. 15, No. 12, December 1977, pp. 1728-1735.

[6]Whitlow, Woodrow, Jr.: XTRAN2L: A Program for Solving the General- Frequency Unsteady Transonic Small Disturbance Equation, NASA TM 85723, November 1983.

[7]Borland, C. J.; and Rizzetta, D. P.: Transonic Unsteady Aerodynamics for Aeroelastic Applications Vol. I--Technical Development Summary, AFWAL TR 80-3107, Vol I, June 1982.

[8]Fuglsang, Dennis F.; and Williams, Marc H.: Non-Isentropic Unsteady Transonic Small Disturbance Theory, AIAA Paper 85-0600.

[9]Hafez, M.; and Lovell, D.: Entropy and Vorticity Corrections for Transonic Flows, AIAA Paper 83-1926.

[10]Hafez, M.; Whitlow, W., Jr.; and Osher, S.: Improved Finite Difference Schemes for Transonic Flow Calculations, AIAA Paper 84-0092.

[11]Osher, S.; Hafez, M.; and Whitlow, W., Jr.: Entropy Condition Satisfying Approximations for the Full Potential Equation of Transonic Flow, Mathematics of Computation, Vol. 44, January 1985, pp. 1-30.

[12]Bridgeman, J. O.; Steger, J. L.; and Caradonna, F. X.: A Conservative Finite Difference Algorithm for the Unsteady Transonic Potential Equation in Generalized Coordinates, AIAA Paper 82-1388.

[13]Steger, J. L.: Implicit Finite Difference Solution of Flow about Arbitrary Two-Dimensional Geometries, AIAA Journal, Vol. 16, No. 7, July 1978, pp. 679-686.

[14]Sorenson, R. L.: A Computer Program to Generate Two-Dimensional Grids about Airfoils and Other Shapes by Use of the Poisson's Equation, NASA TM 81198, May 1981.

[15]Shankar, Vijaya; Ide, Hiroshi; and Gorski, Joseph: A Fast, Time-Accurate Unsteady Full Potential Scheme, AIAA-85-1512-CP.

[16]Shankar, V.; and Ide, Hiroshi: Treatment of Steady and Unsteady Flows Using a Fast, Time-Accurate Full Potential Scheme, AIAA Paper 85-4060.

[17]Jameson, Antony: Solution of the Euler Equations for Two Dimensional Transonic Flow by a Multigrid Method, Princeton University MAE Report No. 1613, June 1983.

[18]Landon, R. H.: NACA 0012. Oscillatory and Transient Pitching, Compendium of Unsteady Aerodynamic Measurements, AGARD Report No. 702, August 1982.

[19]Malone, J. B.; and Sankar, N. L.: Numerical Simulation of Two-Dimensional Unsteady Transonic Flows Using the Full-Potential Equation, AIAA Journal, Vol. 22, No. 8, August 1984, pp. 1035-1044.

[20]Zwaan, R. J.: NLR 7301 Supercritical Airfoil Oscillatory Pitching and Oscillating Flap, Compendium of Unsteady Aerodynamic Measurements, AGARD Report No. 702, August 1982.
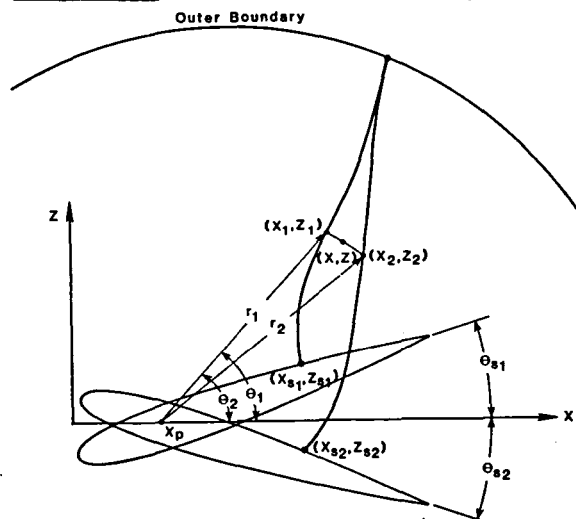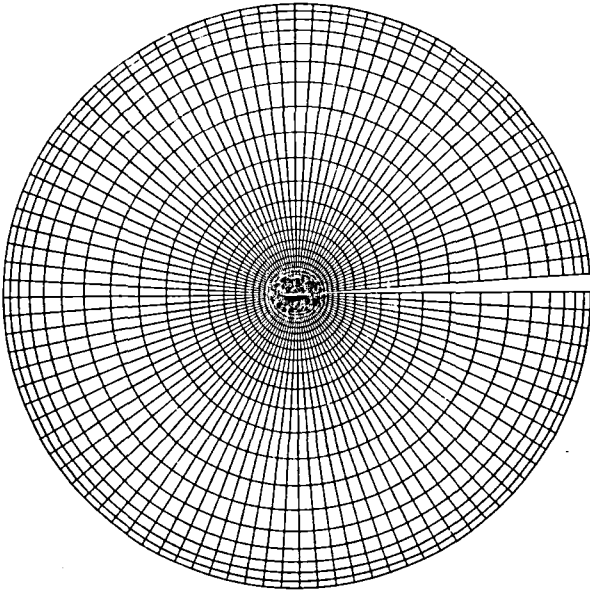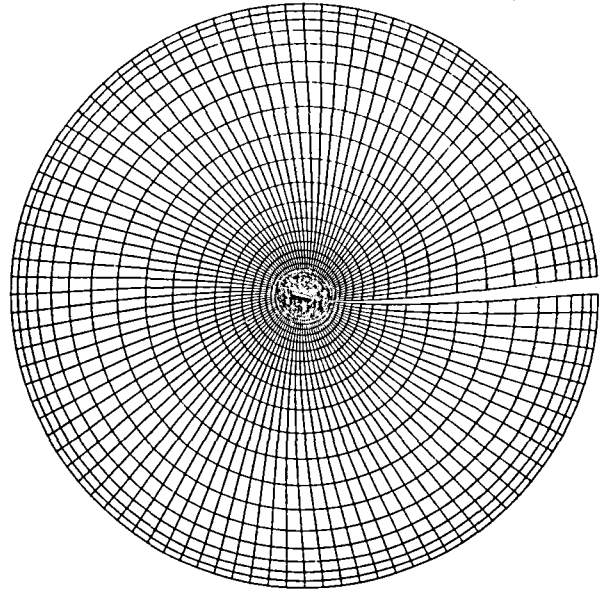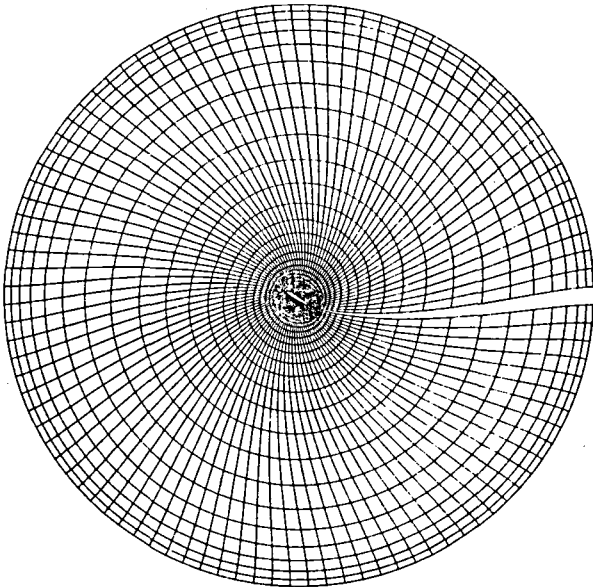
Figure 1. Grid interpolation method.
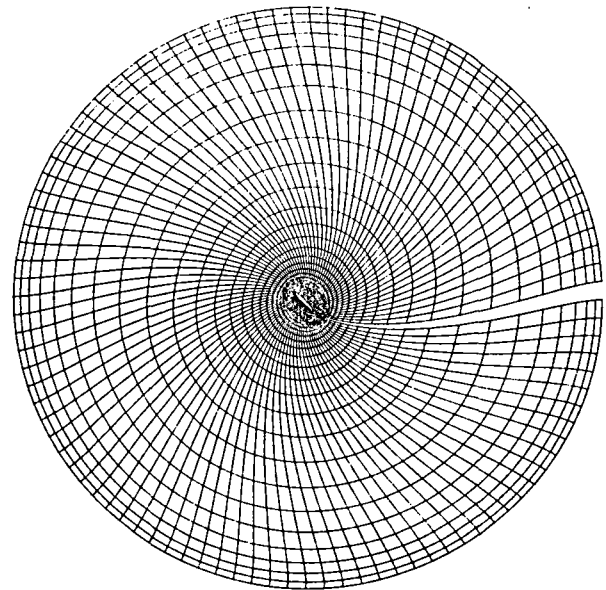
a) Calculated grid, $\alpha = 0^o$

b) Interpolated grid, $\alpha = 15^o$

c) Interpolated grid, $\alpha = 30^o$

d) Calculated grid, $\alpha = 45^o$
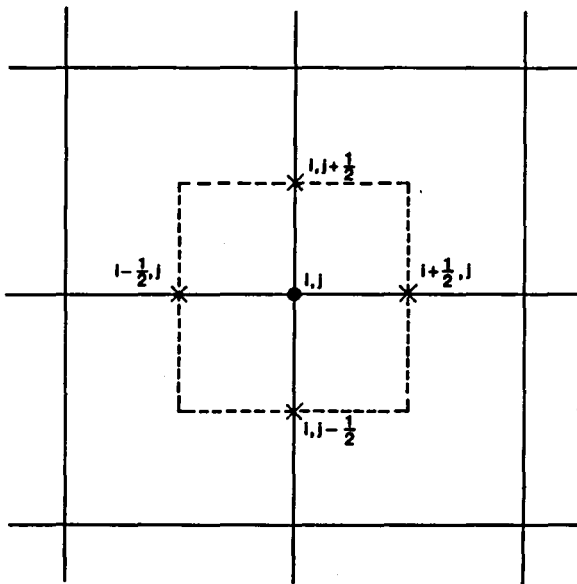
Figure 2. Example of grid interpolation.

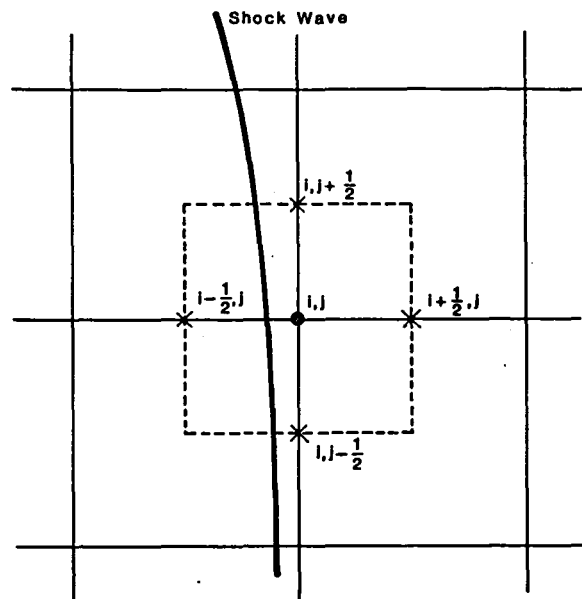Figure 3. Computational cell in interior of flow field.

Figure 4. Computational cell at shock points.
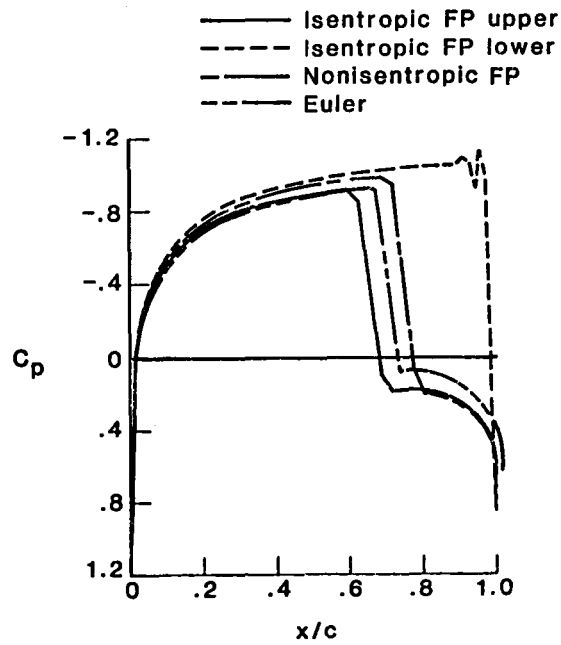

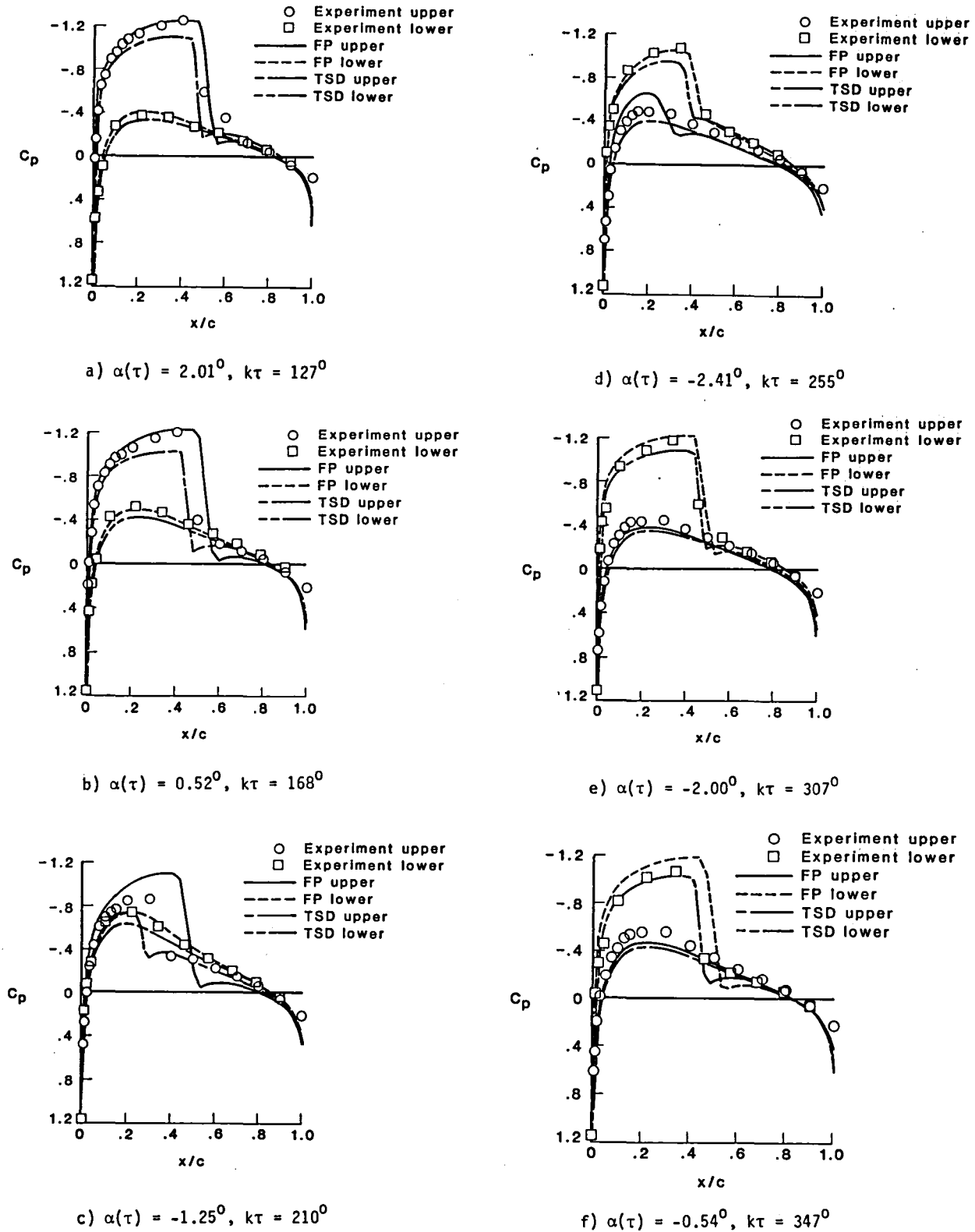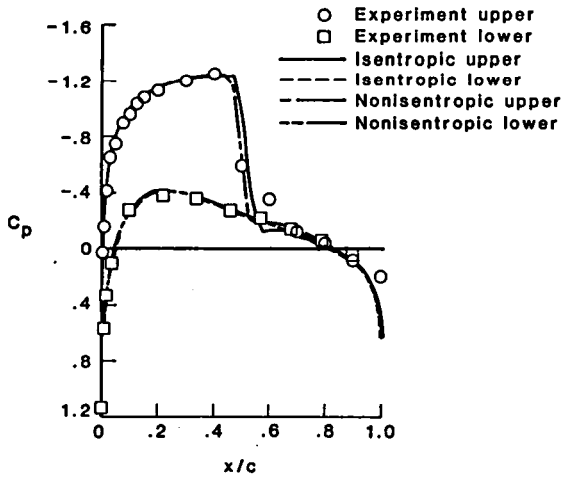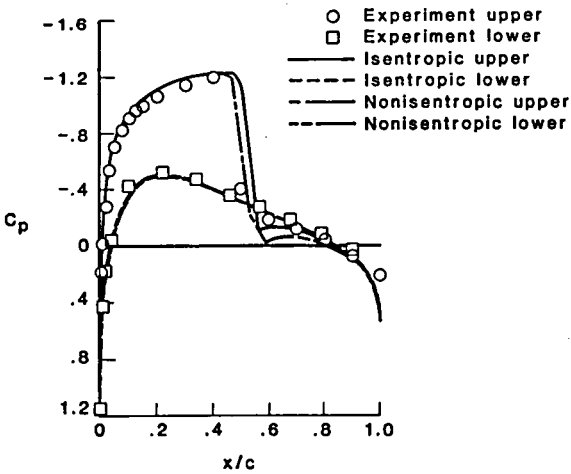Figure 5. Numerical solutions of steady flow past an NACA 0012 airfoil, $M_\infty = 0.84$, $\alpha = 0^0$.
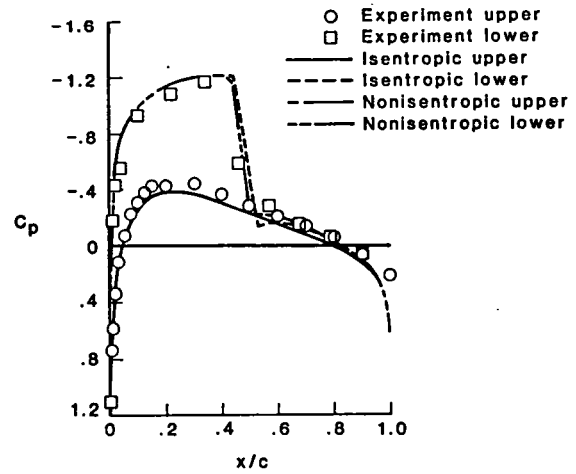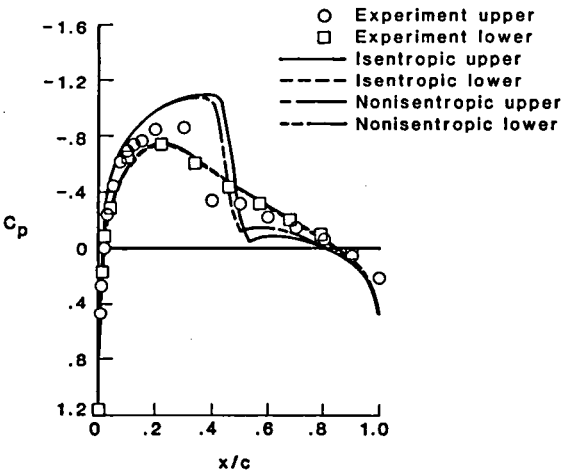
9

a) $\alpha(\tau) = 2.01^{\circ}$, $k\tau = 127^{\circ}$

b) $\alpha(\tau) = 0.52^{\circ}$, $k\tau = 168^{\circ}$

c) $\alpha(\tau) = -1.25^{\circ}$, $k\tau = 210^{\circ}$

d) $\alpha(\tau) = -2.41^{\circ}$, $k\tau = 255^{\circ}$

e) $\alpha(\tau) = -2.00^{\circ}$, $k\tau = 307^{\circ}$

f) $\alpha(\tau) = -0.54^{\circ}$, $k\tau = 347^{\circ}$

Figure 6. Isentropic unsteady pressure vs. experiment for an NACA 0012 airfoil oscillating in pitch, $M_{\infty} = 0.755$, $\alpha(\tau) = 0.016^{\circ} + 2.51^{\circ}\sin(k\tau)$.

10
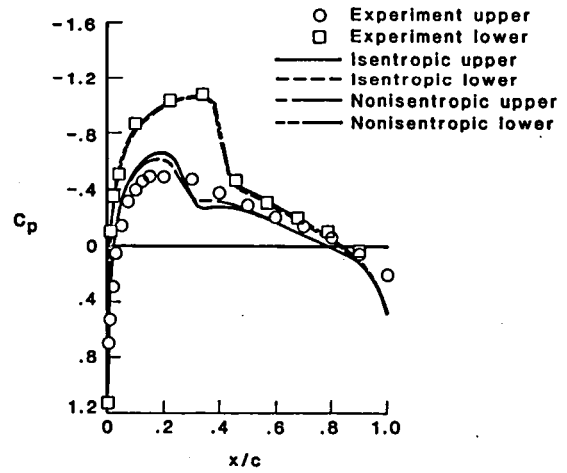
a) $\alpha(\tau) = 2.01^{\circ}$, $k\tau = 127^{\circ}$

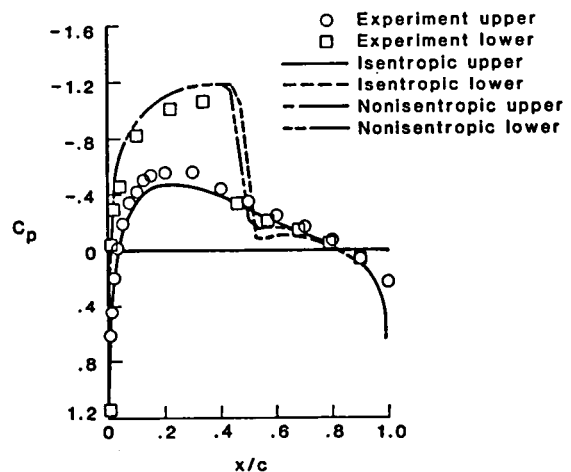d) $\alpha(\tau) = -2.41^{\circ}$, $k\tau = 255^{\circ}$

b) $\alpha(\tau) = 0.52^{\circ}$, $k\tau = 168^{\circ}$

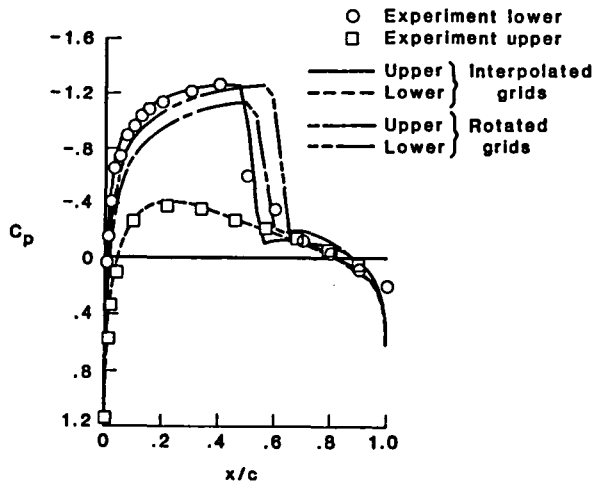e) $\alpha(\tau) = -2.00^{\circ}$, $k\tau = 307^{\circ}$

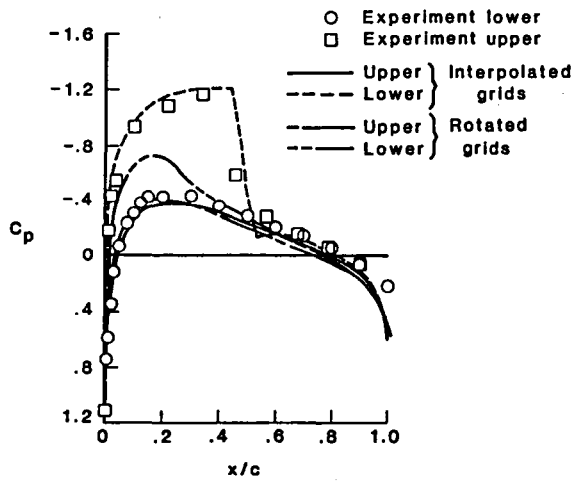c) $\alpha(\tau) = -1.25^{\circ}$, $k\tau = 210^{\circ}$

f) $\alpha(\tau) = -0.54^{\circ}$, $k\tau = 347^{\circ}$

Figure 7.   Isentropic and nonisentropic unsteady pressure vs. experiment for an
NACA 0012 airfoil oscillating in pitch, $M_{\infty} = 0.755$, $\alpha(\tau) = 0.016^{\circ} + 2.51^{\circ}\sin(k\tau)$

11

a) $\alpha(\tau) = 2.01^{\circ}$, $k\tau = 127^{\circ}$

b) $\alpha(\tau) = -2.00^{\circ}$, $k\tau = 307^{\circ}$

Figure 8. Unsteady pressures on an NACA 0012 airfoil calculated using interpolated and rotated grids, $M_{\infty} = 0.755$,

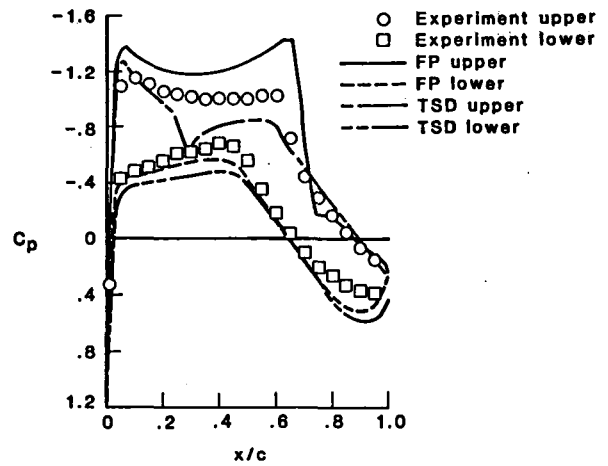$\alpha(\tau) = 0.016^{\circ} + 2.51^{\circ}\sin(k\tau)$.

Figure 9. Isentropic steady pressures vs. experiment for an NLR 7301 airfoil, $M_{\infty} = 0.721$, $\alpha = -0.19^{\circ}$.
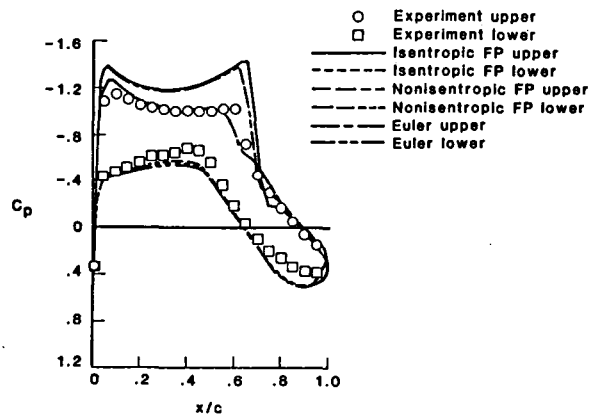

Figure 10. Isentropic and nonisentropic steady pressures vs. experiment for an NLR 7301 airfoil, $M_{\infty} = 0.721$, $\alpha = -0.19^{\circ}$.

1. Report No.	2. Government Accession No.	3. Recipient's Catalog No.
NASA TM-87769		

4. Title and Subtitle	5. Report Date
AN ENTROPY CORRECTION METHOD FOR UNSTEADY FULL POTENTIAL FLOWS WITH STRONG SHOCKS	June 1986
	6. Performing Organization Code
	505-63-21-01

7. Author(s)	8. Performing Organization Report No.
Woodrow Whitlow, Jr.; Mohamed M. Hafez*; and Stanley J. Osher**	
	10. Work Unit No.

9. Performing Organization Name and Address	
NASA Langley Research Center Hampton, VA 23665-5225	11. Contract or Grant No.
	13. Type of Report and Period Covered

12. Sponsoring Agency Name and Address	Technical Memorandum
National Aeronautics and Space Administration Washington, DC 20546-0001	14. Sponsoring Agency Code

15. Supplementary Notes

16. Abstract

An entropy correction method for the unsteady full potential equation is presented. The unsteady potential equation is modified to account for entropy jumps across shock waves. The conservative form of the modified equation is solved in generalized coordinates using an implicit, approximate factorization method. A flux-biasing differencing method, which generates the proper amounts of artificial viscosity in supersonic regions, is used to discretize the flow equations in space. Comparisons between the present method and solutions of the Euler equations and between the present method and experimental data are presented. The comparisons show that the present method more accurately models solutions of the Euler equations and experiment than does the isentropic potential formulation.

17. Key Words (Suggested by Author(s))	18. Distribution Statement
Nonisentropic Full Potential Unsteady Entropy Corrections Flux Biasing	Unclassified - Unlimited Subject Category 02

19. Security Classif. (of this report)	20. Security Classif. (of this page)	21. No. of Pages	22. Price
Unclassified	Unclassified	13	A02

N-305

End of Document